Post test Analyses of the NESC II Experiments on Cladded Cylinders with Circumferential Cracks subjected to a Pressurized Thermal Shock

Matthias Fischer[1], Surender Bhandari[1] and Eberhard Roos[2]

1) Framatome ANP, Paris La Défense, France
2) MPA Stuttgart, Germany

ABSTRACT

In the framework of the European Commission 2nd Project on Network for the Evaluation of Structural Components - NESC II - two experiments have been carried out at MPA Stuttgart, on cladded cylinders with two types of cracks on the internal surface:

- One fully circumferential under-clad crack of depth 8 mm
- Two elliptical through-clad surface cracks of depth about 20 mm, aspect ratio (length/depth) of about 3, situated one opposite the other on the circumference.

In both cases, the applied loading consists of internal pressure, an axial load and a thermal shock induced with the injection of cold water on the heated cylinder. The material used is a special type of alloy developed in Germany, which has low toughness characteristics and thus simulates the end-of-life toughness properties of a nuclear reactor pressure vessel. The tests thus represent a PTS transient applied to a RPV under the EOL material properties. In the first test (NP2), the fracture initiation took place and the crack arrested after a stable growth of about 8 mm. In the second test (NP1), the fracture initiation event did not take place.

This paper presents the post-test analyses of these experiments, conducted using the SYSTUS-code. It is shown that in both the cases, the analyses predict the results obtained experimentally.

INTRODUCTION

In this document, posttest analyses of the NESC II experiments [1] are discussed. These experiments on a cladded cylinder under thermal shock loading were performed at MPA Stuttgart. The NP1 test piece contains two elliptic through-clad cracks. In the NP2 test a fully circumferential crack under the cladding is examined. The calculations presented in this paper were performed on both experiments NP1 and NP2 at Framatome with the finite element program SYSTUS [2].

GEOMETRY OF TEST SPECIMENS

For both tests, NP 1 and NP 2, the same test specimen is used. The geometry of the test cylinder is given in Figure 1. The defect geometry is different in the two tests and will be presented later.

MATERIAL PROPERTIES

In the NP1 and NP2 experiments, 17 Mo V 8 4 material cylinders with an austenite cladding were used. The material properties are provided in [1] and will not be repeated here. One must mention, however, that for the simulation with SYSTUS some of the data had to be modified slightly as indicated below. Moreover, for the rest material (see figure 1), only Young's modulus is specified. Therefore, all remaining parameters of the rest material are assumed to be same as that of the base material.

Reference temperature for the thermal expansion coefficient is 35 °C. In the finite element programme SYSTUS the reference temperature is fixed at 0 °C. However, the given expansion-temperature-curve can be assumed linear in the low temperature range. Thus, the influence of the reference temperature is a constant offset in the thermal strains. For the SYSTUS analysis, the base material is loaded with an initial deformation to give zero thermal strains at 35 °C. As for the thermo-physical properties of the cladding material, the reference temperature for the thermal expansion coefficient is not known. In the simulation, it is assumed to be 0 °C. The initial deformation of the cladding material is chosen according to the specifications to give no thermal stresses at 300 °C.

Mechanical properties

Young's modulus E at different temperatures for the cladding, base and rest material is given in [1]. Poisson's ratio is assumed constant at 0.3. In SYSTUS code, the hardening curve for an elasto-plastic calculation has to be given in true stress–true plastic

strain. For different temperatures, it is mandatory to give the corresponding values of true stress at the same true plastic strains. Thus, it was necessary to make a modified interpolation of the original elasto-plastic properties for use in the analysis code.

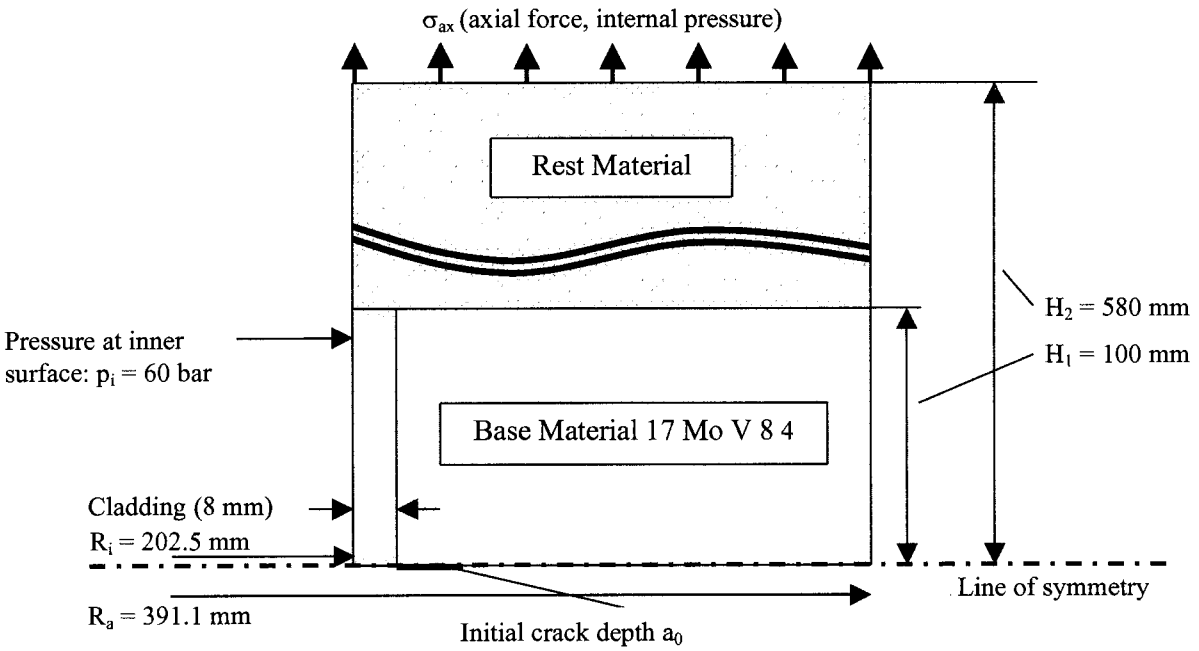

Figure 1: Geometry of test cylinder in NP1 and NP2 test

ANALYSIS OF NP2 TEST

Defect geometry and finite element modelling

NP2 has one fully circumferential crack under the cladding. The crack depth ranges from 6.0 to 10.5 mm along the circumference with an averaged value of 8.0 mm. In this analysis, the influence of the changing crack depth is neglected. For the simulation of the NP2 experiment an axisymmetric finite element model is used. It consists of rectangular and triangular elements with quadratic form functions. At the crack tip the element size is 0.5 x 0.5 mm^2. Figure 2 shows a detail of the FE mesh that is employed in the analysis.

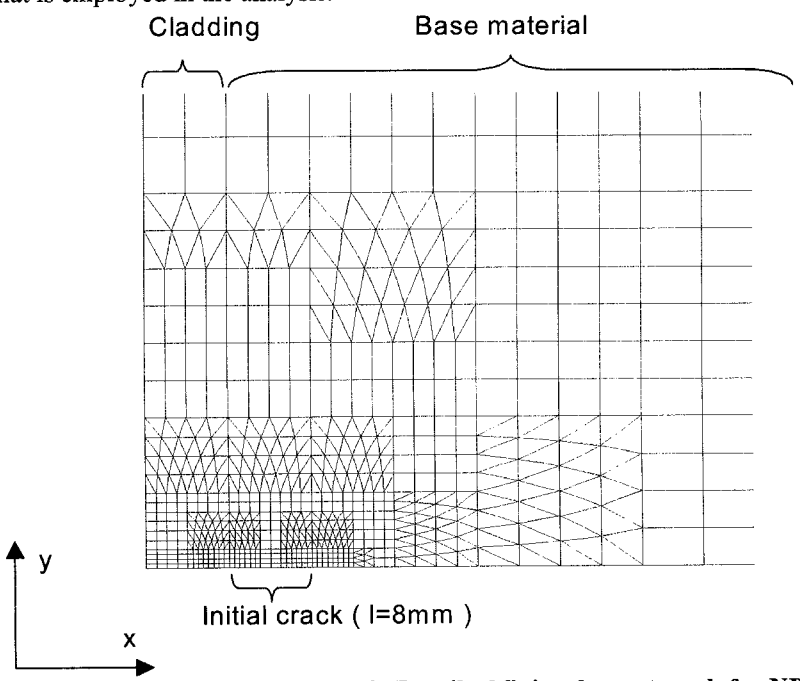

Figure 2: Detail of finite element mesh for NP2 simulation

Thermal analysis

Initial condition: At time t=0, steady state is assumed. The temperature distribution in each radial plane is constant in axial direction. As per the specification [1], a temperature of T_i=234.8 °C and T_O=287.1 °C is imposed on the inner and outer surface, respectively.

Boundary conditions: Thermal boundary conditions during the thermal shock on the inner and outer surface of the tube are given in [1]. Linear interpolation between the given values is used. Thermal shock loading on the inside of the tube starts at 15 seconds. Heat flow on the upper and lower surface is assumed zero to assure a constant temperature profile in axial direction.

Results: The radial temperature distribution in the tube wall is computed for different times during the experiment. Due to the large heat transfer, the temperature on the inner wall surface drops rapidly. The temperature on the outer surface changes little. The temperatures calculated in the middle of the tube wall correspond well to the experimental results. On the surfaces and within the cladding there are some differences between test and simulation. Figure 3 shows a comparison of calculated and measured temperature values for different radial positions. The small increase of inner surface temperature at the beginning of the experiment is due to the retarded start of the thermal shock at 15 seconds.

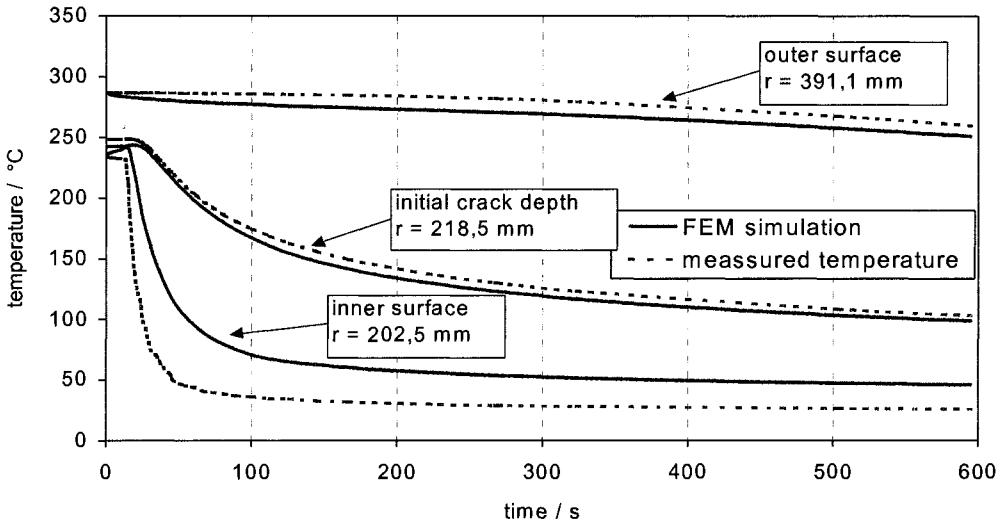

Figure 3: Comparison between calculated and measured temperature data

The calculated temperature on the inner wall surface is significantly higher than the measured wall temperature. Thus, the average radial temperature gradient in the simulation between the inner surface and the crack tip is smaller than in the experiment. This results in a lower loading of the crack tip during the thermal shock and has to be kept in mind when interpreting the results of the mechanical analysis. However, the local temperature gradient at the crack tip is approximately the same in experiment and simulation.

As for the temperature difference between the inner tube surface or the interface and the crack tip, it increases very fast at the beginning of the thermal shock. It reaches a maximum of ΔT=103 K at t=65 s between the surface and the crack tip. This value corresponds to an average radial temperature gradient of 6.5 K/mm. Measurements during the experiment showed a maximum temperature difference of more than 160 K.

Mechanical analysis

Boundary conditions and loading: The mechanical analysis is performed with a crack length of 8.0 mm. The nodes on the crack surface are not restricted. The remaining nodes in the symmetry line of the tube are fixed in y-direction. On the inside of the tube, a pressure of p_i=5.8 MPa is applied. On the upper surface a pressure of p_u=124.4 MPa is applied to account for the axial Force F_{ax}=43 MN and the internal pressure p_i. The outside of the tube is a free surface.

The residual stresses in the cladding are modelled by an initial deformation of the elements. It is chosen to give zero thermal stresses at 300 °C. As mentioned earlier, the thermal deformation in the base material is assumed to be zero at 35 °C. The calculated axial residual stress in the cladding at reference temperature of 35 °C is 275 MPa. This corresponds to the experimental findings. Prior to the test, residual stress was measured using bore-hole technique. The average axial component was found to be 224 MPa.

Results: The axial strain on the inner and outer tube surface for the cracked cross section have been evaluated. On the internal side (cladding), one obtains a steep increase of strain during the thermal shock. This is caused by the fast increasing spatial temperature gradient. As for the plastic deformation at the crack tips during the thermal shock at 100 seconds, it is noticed that towards the base material, it is restricted to a small zone around the crack tip. Within the softer cladding material, high plastic deformation up to 10% is encountered and plastification occurs throughout the ligament.

Fracture analysis

The high plastic deformation in the cladding material will influence the loading of the crack tips on both sides, in the cladding as well as in the base material. Thus, a linear-elastic fracture mechanics analysis would not lead to a correct characterisation of the crack tip loading. In this section results obtained by the elasto-plastic G-Theta approach [3] are presented for the initial crack length of 8.0 mm.

In the G-Theta approach the energy release rate is calculated by applying virtual displacements on the crack front. For linear elasticity the relation between the energy release rate and stress intensity factor is given by:
$G=J=K_I^2/E^*$, where J is Rice Integral, E^* is Young's modulus E for plane stress and $E/(1-\nu^2)$ for plane strain. Thus K_J can be calculated in an elasto-plastic analysis as $K_J^2=E^*G$. Here, plane strain conditions are assumed.

The crack driving force profile for the NP2 test with an initial crack length of 8 mm is shown in Figure 4. It is compared to fracture toughness data for the base material used in the NESC II experiments given in [4].

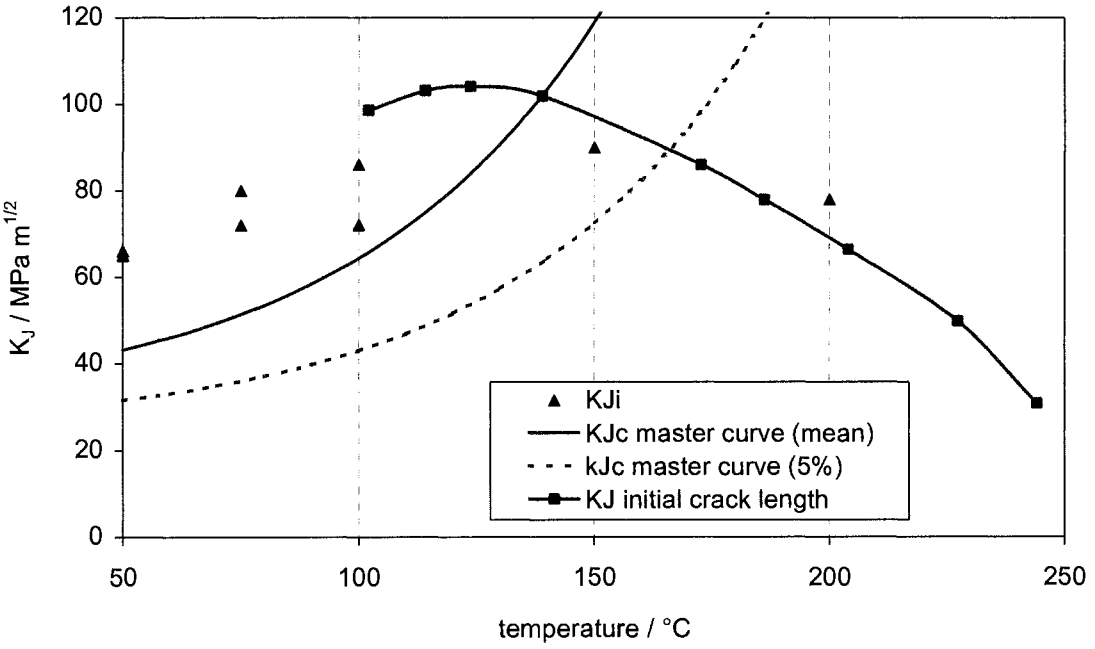

Figure 4: Crack driving force in NP2 test

A master curve analysis on the available fracture data was performed by David Swan [5]. The critical fracture toughness values determined on test specimens with crack front length B1 are size corrected according to the defect front length B2 (crack front length in NP2 test B2=1373mm):

$$K_{B2} = 20 + (K_{B1} - 20) \times \left(\frac{B1}{B2} \right)^{1/4} \quad (1)$$

The expressions for the mean and lower 5% bound are given by:

$$K_{Jc} = 30 + 70 \times \exp[0.019 \times (T - T_0)) \quad \text{mean} \quad (2)$$

$$K_{Jc} = 24.5 + 37.8 \times \exp[0.019 \times (T - T_0)) \quad \text{lower 5\% bound} \quad (3)$$

where T is the temperature at the crack tip and T_0 is the reference temperature. For the defect front length of 1373 mm in the NP2 experiment, the reference temperature is given by T_0=137.37 °C.

The initiation toughness K_{Ji} for temperatures above 100 °C is in the range of 80-110 MPa $m^{1/2}$. These values must not be size corrected. According to the fracture toughness data, crack initiation is predicted in a temperature range between 150 °C and 130 °C at the crack tip which corresponds to t=150 s and t=250 s, respectively during the experiment. This result correlates well with the experimental observations. In the experiment, crack initiation was detected at t=186 s. The temperature of the crack tip was 142.4 °C at crack initiation.

Crack growth: During the NP2 experiment, crack growth was observed. In order to specify the load on the enlarged crack, a simulation was performed with a total crack length of 20 mm, i. e. crack growth of 12 mm. Figure 5 shows a comparison of the crack driving force profiles for the initial crack length of 8 mm and a crack length of 20 mm.

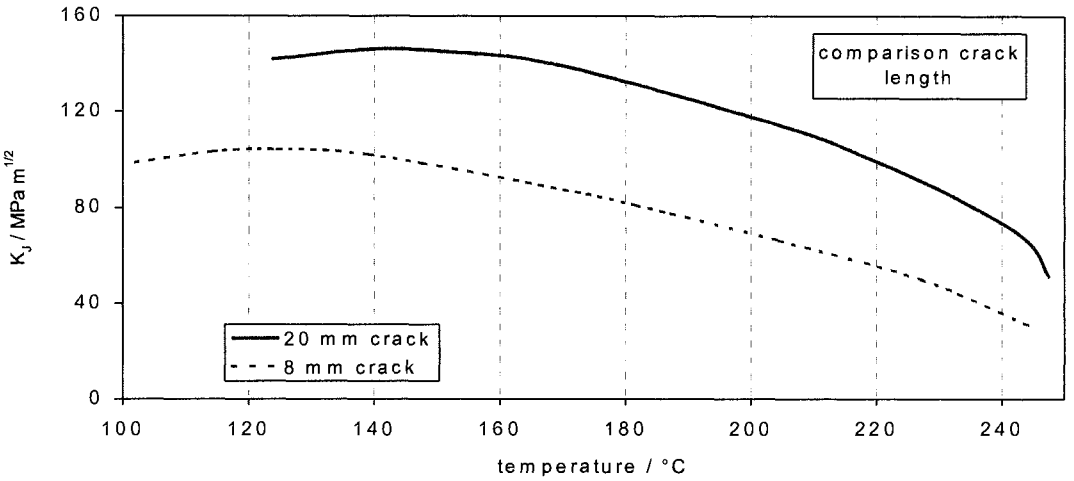

Figure 5: Crack driving force for 8 mm and 20 mm crack

For a crack length of 20 mm, the crack driving force profile shows a higher maximum at a higher temperature compared to the initial crack length. Crack arrest cannot be predicted in the analysis since no material data is available.

ANALYSIS OF NP1 TEST

Defect geometry and finite element modelling

The NP1 test specimen has two elliptic through-clad cracks. They have been inserted in the circumferential plane on the inner surface of the tube on opposite sides. The crack geometry is given in Table I

Table I: Dimension of defects in specimen NP1

	Total crack depth d / mm	Total crack length 2c / mm
defect A	23,8	63
defect B	19,6	59

A three-dimensional finite Element analysis is performed. The size of the two defects is similar which allows to assume symmetry. Thus, only one eighth of the tube is modelled. The finite element mesh for defect A is shown in Figure 6. It contains 5937 nodes and 1747 elements with quadratic form functions.

For modelling the finite element mesh around the crack tip, the SYSTUS toolbox BLOC [7] was used. An option of BLOC allows to construct through-clad cracks. The crack front consists of straight lines in the cladding and an ellipse in the base material.

Figure 6 also shows the finite Element mesh on the crack surface of defect A created with BLOC. Due to the restrictions of BLOC, the crack form is slightly altered compared to the problem definition in [1]. The values of the dimensions c and d correspond precisely to the problem definition.

Along the crack front a 4-layer radial expanding mesh is employed, see Figure 6. The size of the elements is 0.3 mm at the crack tip. The intermediate nodes of the first layer are placed at a distance of a quarter element size to achieve a

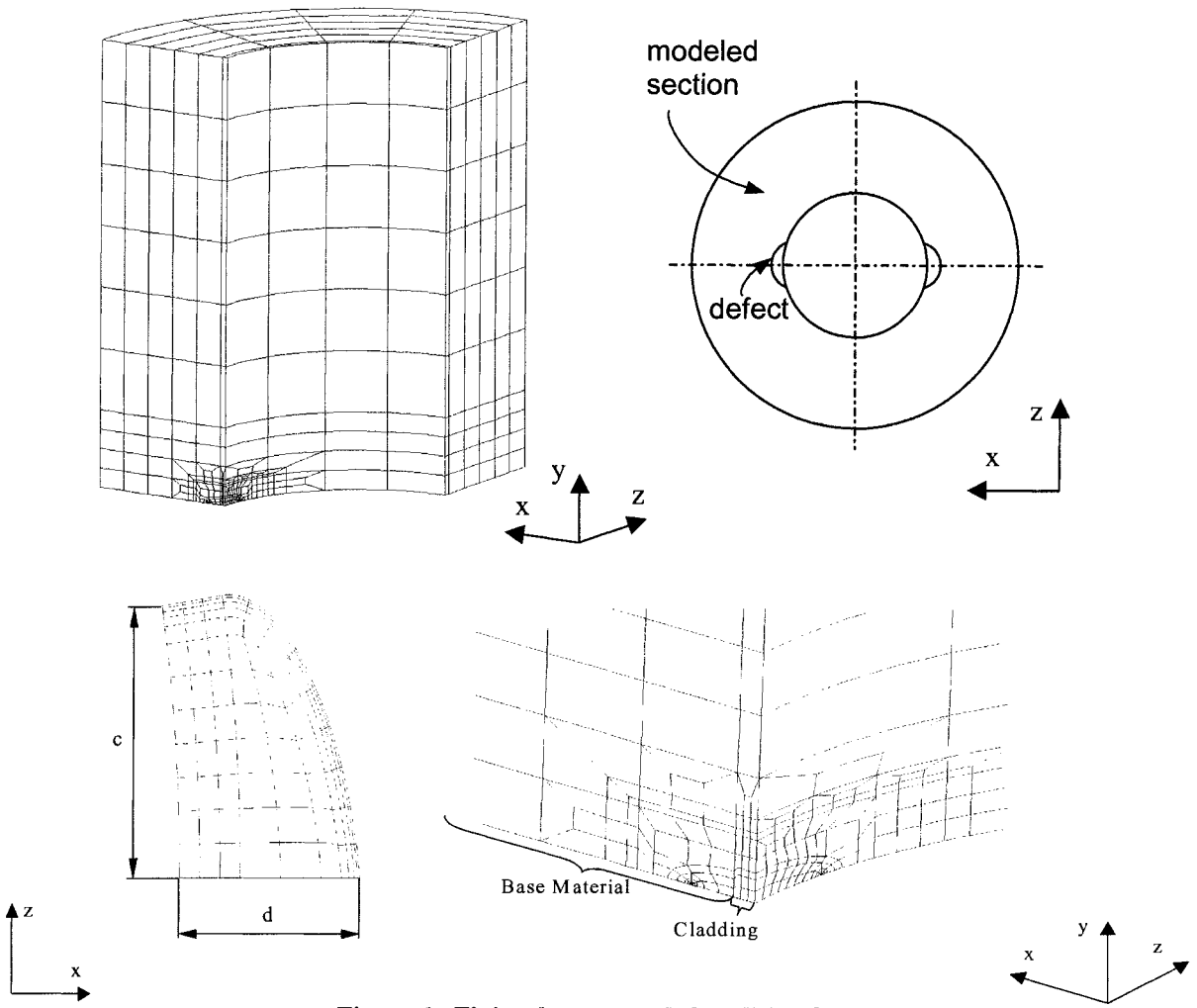

Figure 6: Finite element mesh for NP1 defect A

better approximation of the elastic singularity at the crack tip.

Thermal analysis

Initial condition: At time t=0, steady state is assumed. The temperature distribution in each radial plane is constant in axial direction. As per the specification, a temperature of T_i=155 °C and T_O=200 °C is imposed on the inner and outer surface, respectively.

Boundary conditions: Thermal boundary conditions during the thermal shock on the inner and outer surface of the tube are given in [1]. Heat flow on the upper and lower surface is assumed to be zero.

Results: A comparison between measured and calculated temperatures for the NP1 test is shown in Figure 7. One notices that – as in the NP2 test - the calculated values on the inner surface do not fit the measured temperatures. Within the tube wall, the simulation approximates the measured temperature distribution quite well.

During the thermal shock, the temperature in the tube close to the inner surface decreases rapidly. This gives rise to a high temperature gradient in radial direction. A maximum temperature difference of ΔT=60 K between surface and crack front (deepest point) is encountered between t=40 s and t=60 s. This corresponds to an average gradient of 3 K/mm. Comparing this with the temperature difference in the NP2 test, one finds a lower thermal loading in NP1 test.

Mechanical analysis

Boundary conditions and loading: The cracked cross section of the tube is a symmetry plane of the finite element model. The nodes in this plane are fixed in axial direction except for the nodes on the crack surface. The nodes on the remaining two symmetry planes of the 1/8 tube model are fixed in x- and z-direction, respectively.

On the inside of the tube and on the crack surface, a pressure of p_i=7.8 MPa is applied. On the upper surface a pressure of p_u=59.7 MPa is applied to account for the axial Force F_{ax}=20 MN and the internal pressure p_i. The outside of the tube is a free surface. Initial deformation is applied on the elements to account for residual stresses between cladding and base material. As for the NP2 test, stress free temperature is chosen at 300 °C.

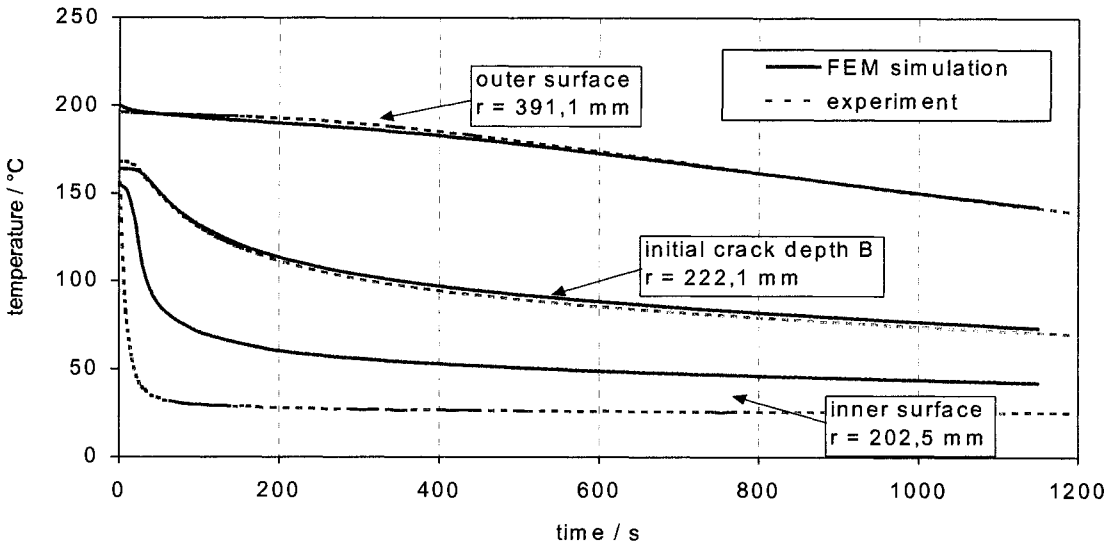

Figure 7: Calculated and measured temperatures for NP1 test

Fracture analysis

The crack driving force profiles for the NP1 test were calculated using the G-Theta approach as described earlier. In Figure 8, the calculated crack driving force profiles for defect A and B are compared to fracture toughness data. The defect length for the cracks in the NP1 test is 60 mm which corresponds to a reference temperature of T_0=74.45 °C for the critical fracture toughness master curve [5].

The maximum stress intensity factor is similar for both defects. The profile for crack B is shifted to a lower temperature due to the smaller crack depth. In Figure 8, it can clearly be seen that for both defects the finite element simulation predicts no crack initiation.

Fracture analysis with increased axial load

A finite element analysis with increased axial force is performed to answer the question if crack initiation could have occurred in NP1 test with higher mechanical loading. Figure 9 shows the crack driving force profile for defect B for the maximum axial load of 100 MN.

With an axial load of 100 MN, the calculated stress intensity factors are higher than with the experimental setup of 20 MN. The crack driving force profile passes the scatter of crack initiation values. The mean bound of the cleavage toughness master curve is crossed after the maximum of the crack driving force profile. Thus, crack initiation and some limited crack growth should occur.

However, the mechanical part of the loading would be very high and crack initiation would be caused immediately by the axial load and not by the thermal shock. Furthermore, crack initiation would occur at high temperatures on the upper shelf of the fracture toughness values. Thus, a test design with an axial load of 100 MN would not correspond to the target of NP1 test to examine crack initiation by thermal shock in the transition region of the fracture toughness curve.

CONCLUSIONS

The SYSTUS post test analyses of the NESC II experiments give the following results:

-Crack initiation for the circumferential crack in NP2 test is predicted between t=150 s and t=250 s during the thermal shock.
-No crack initiation is predicted for the elliptic through-clad cracks in NP1 test.

Both the simulation results correspond to the experimental observations in the NP1 and NP2 tests that were performed at MPA Stuttgart.

A further analysis of NP1 test shows that an increased axial load might lead to crack initiation due to mechanical loading at temperatures in the regime of upper shelf fracture toughness data.
Prediction of crack growth in the NP2 experiment is not made since no material data is available.

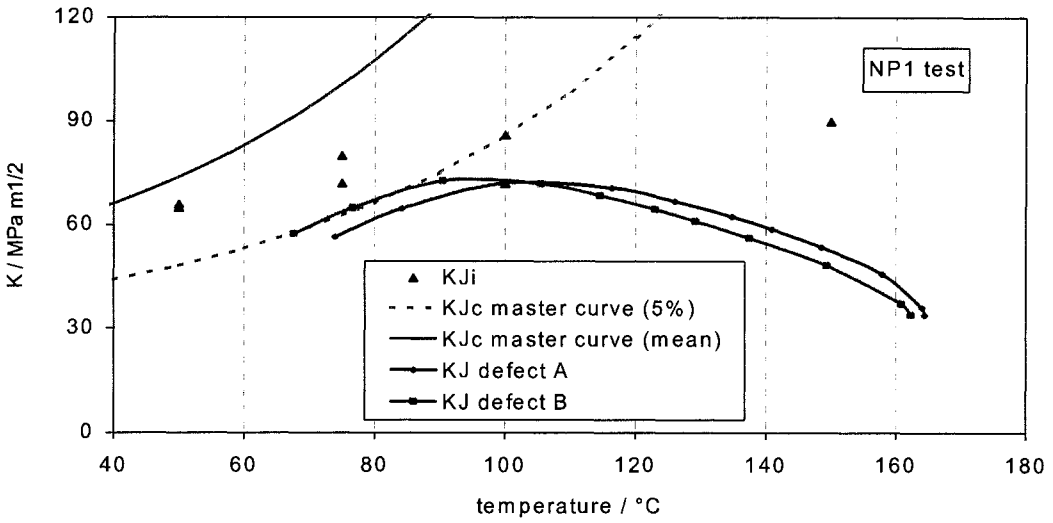

Figure 8: Crack driving force in NP1 test

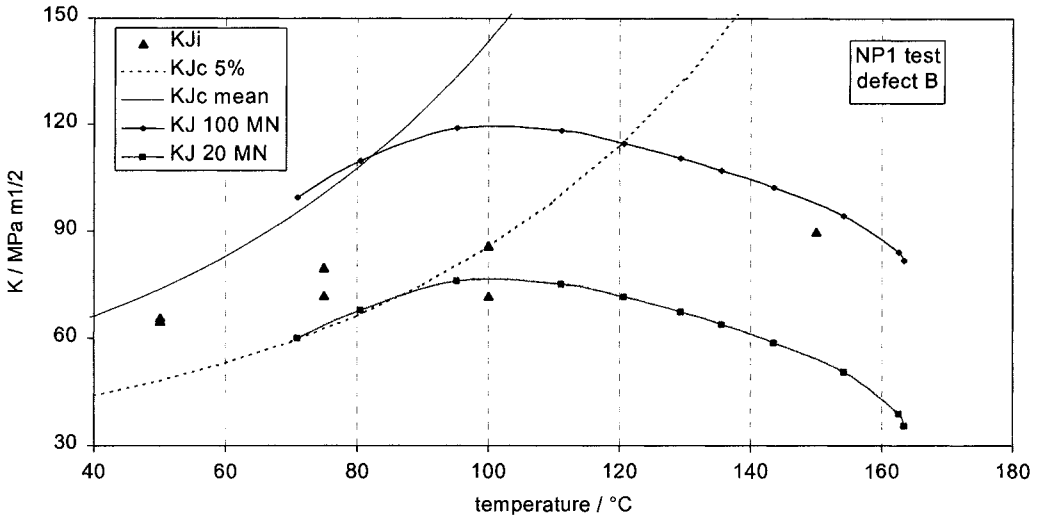

Figure 9: Crack driving force for defect B with increased axial load (F_{ax}=100 MN)

REFERENCES

1. Stumpfrock L. and Taylor N. : NESC II Post Test Structural Analysis Problem Definition Document. NESC TG3 DOC, JRC-Petten, The Netherlands, March 2000.
2. SYSTUS International: SYSTUS '99 Manuel de Référence Analyse. Lyon (France).
3. SYSTUS International: SYSTUS '99 Manuel de Référence - Mécanique de la Rupture. Lyon (France).
4. Stumpfrock L. and Taylor N : NP1 Structural Analysis Problem Definition Document. NESC TG3 DOC (99) 04, JRC-Petten, The Netherlands, June 1999.
5. Swan D. I. : NESC II Project – Analysis of Toughness Data. Personal communication, March 2000.
6. Règles de Surveillance en Exploitation des matériels Mécaniques des îlots Nucléaires REP (RSE-M). AFCEN, Paris, Modification December 1999.
7. Mourgue Ph. : Notice d'utilisation des outils développés dans le cadre des actions R&D BLOC FISSURE en 1999. Systus International, January 2000.